Spring 2022

Interfacial Electrochemistry in Metallic Film Fabrication

Eric S. Tuala
Eastern Illinois University

INTERFACIAL ELECTROCHEMISTRY IN METALLIC FILM FABRICATION

Eric S. Tuala

Department of Chemistry & Biochemistry

Eastern Illinois University

Spring 2022

Abstract

An experimental determination of RC constant at the edge and the center of a disk electrode was done using *in situ* reflectance spectroscopy on a Au electrode immersed in $HClO_4$ as electrolyte. The RC constant at the edge of the disk electrode was found much smaller than that at the center. Such differences contribute to the selective removal of the deposited Cu on an Au disk electrode.

Furthermore, the electrochemical corrosion of Cu^{2+} towards Co electrode (called cementation reaction) was investigated using a Co/Pt rotating disk electrode. The Open Circuit Potential of Co electrode in $CuSO_4$ electrolyte was recorded at different rotation rates. The reaction rates between Cu^{2+} and Co electrode were calculated under different conditions such as the thickness of Co substrate, the concentration of Cu^{2+} in the electrolyte, and the presence of proton (acidic media).

Acknowledgements

First and foremost, I would like to express my sincere gratitude to my advisor Dr. Zhange Feng for accepting this role. His advice, patience, continuous support, motivation, and broad knowledge helped accomplished this MS study and research.

Besides my advisor, I would like to thank the thesis committee: Dr. Gopal Periyannan, Dr. Michael Beck, Dr. Zhiqing Yan for accepting this role, encouragement, and insightful comments.

My special thank should go to the Graduate Coordinator, Dr. Radu Semeniuc for his advice, leadership, and coordination. To all EIU professors, especially the Department of Chemistry and Biochemistry, thank you for the knowledge, explanation, teaching, and coaching during my MS in Chemistry.

I also thank my fellow lab mate in Dr. Feng's group: Pedro Vasquez for helping me while collecting the data.

To my colleagues, my wife, my parents, my sibling, thank you for the support, moral as well as material that helped make this dream come true.

Contents

List of Pictures

List of Figures

1. INTRODUCTION

Several items such as batteries, integrated circuits, transistors, and microchip, are manufactured mainly by exploiting the redox potential between two chemicals either to produce energy (i.e., batteries) or to manufacture a material that conducts electric current (semiconductor). the quest for the miniaturization of electronic devices calls for the manufacture of much more stable materials (thermal stability) and having a low resistivity.

The study of the interface between two chemical compounds (electrode and electrolyte) ready to react via a redox reaction is of utmost importance to be able to understand the conditions under which the two reagents can make it possible to produce materials of superior quality.

Electrochemistry is a discipline of analytical chemistry which makes it possible to investigate two reagents via electroanalytic methods such as chronoamperometry or chronopotentiometry. In this thesis, we conducted investigations on the interface between an electrode and an electrolyte to contribute to the cutting-edge technology on the manufacture of nanomaterials.

1.1. Electroanalytical method

Several electroanalytic methods can be used depending on the data to collect and analyze. In this thesis, we purposely exploited a couple of them using an electrochemical analyzer such as the potentiostat, CHI 660C (CH instrument).

Picture 1: Electrochemical analyzer (potentiostat) CHI 660C.

The electrochemical analyzer is connected to the computer in other to run the experiment and collect data. We can choose the electrochemical technique to use from the dialog box. For each electrochemical technique, we set the parameters with respect to the experiment we run and the data we expect to collect.

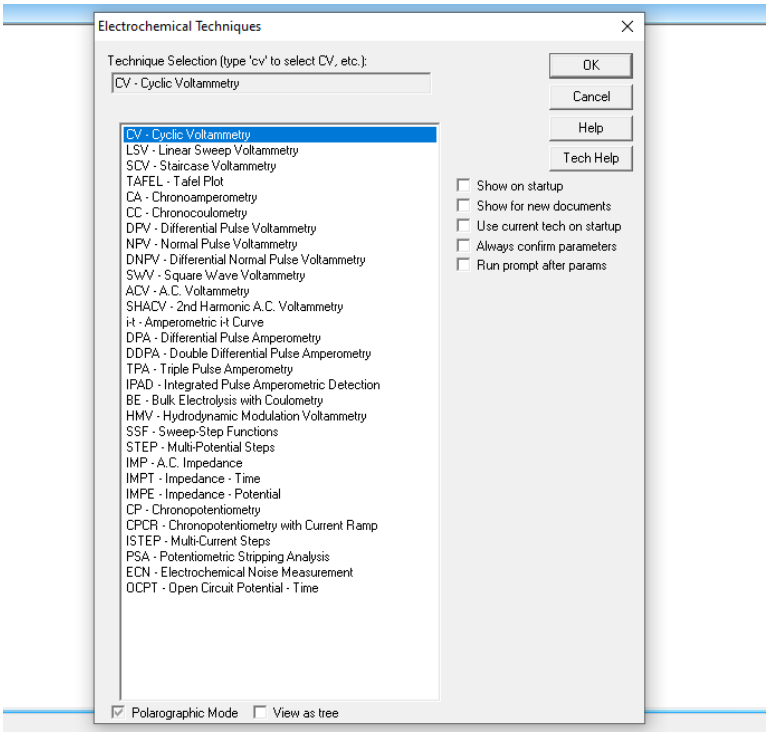

Picture 2: Electrochemical technique box in the potentiostat CHI 660C.

1.1.1. Cyclic Voltammetry (CV)

CV is a multipurpose electroanalytical technique for the study of electroactive species since it can be used in diverse field of chemistry such as electrochemistry, inorganic chemistry, organic chemistry, and biochemistry. As an electrode is immersed in an unstirred solution, CV measures the current drawn by the electrode as its potential changes. Using a saturated calomel electrode (SCE) or a silver/silver chloride electrode (Ag/AgCl) as a reference electrode, the potential of this working electrode is controlled. Excitation signals are generated by applying a controlling potential across these two electrodes. CV uses a linear potential scan with a triangular waveform as the excitation signal[1].

During a potential scan, the current at the working electrode is measured to produce a cyclic voltammogram. The current represents the response to the potential excitation signal. Voltammograms show the relationship between current (vertical axis) and potential (horizontal axis). The horizontal axis is also considered a time axis since the potential varies linearly with time[1].

The parameters to set to run a CV are:

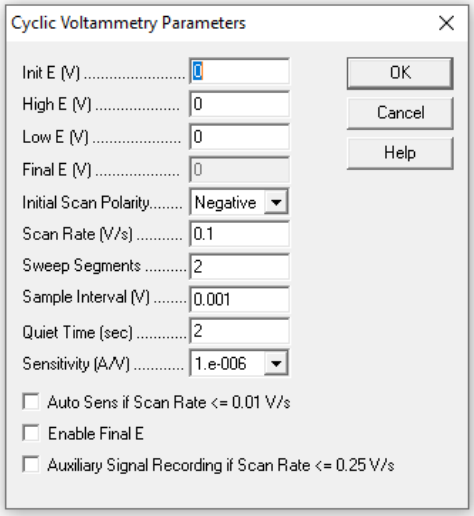

Picture 3: Cyclic voltammetry parameters box in the potentiostat CHI 660C.

1.1.2. Chronoamperometry (CA)

One of the most commonly used voltametric methods is chronoamperometry, although it is one of the simplest. Chronoamperometry, at its most basic level, is the measurement of the current that results from the application of an external voltage at time t_0. As a basic example of voltametric operation, chronoamperometry is an ideal technique to analyze as part of a voltametric analysis.[2]

In chronoamperometry, we measure the current flowing through an electrode as a function of a constant potential applied to the working electrode (in comparison with the reference electrode).[2] The parameters to set to run a CA are:

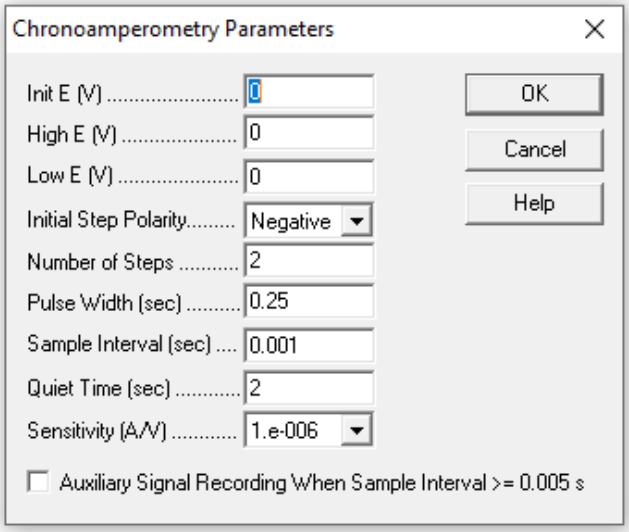

Picture 4: Chronoamperometry parameters box in the potentiostat CHI 660C.

1.1.3. Chronopotentiometry (CP)

With chronopotentiometry, an electrical current is applied to the electrode and the potential changes to a level at which the flux of the electroactive species is enough to supply the current. As a result, after a while, the flux of redox species to the surface is not sufficient to maintain this current, and the potential shifts rapidly from its initial value to that of another species (often a solvent or electrolyte).[3] The parameters to set to run a CP are:

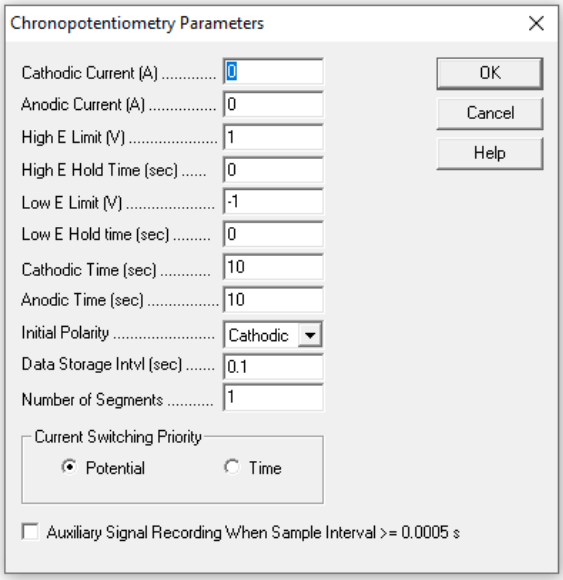

Picture 5: Chronopotentiometry parameters box in the potentiostat CHI 660C.

1.1.4. Open Circuit Potential (OCP)

In an electrode system, the open circuit potential of the working electrode is defined as the potential between it and the environment in relation to a reference electrode, which is placed close to it in the system.[4] The parameters to set to run an OCP are:

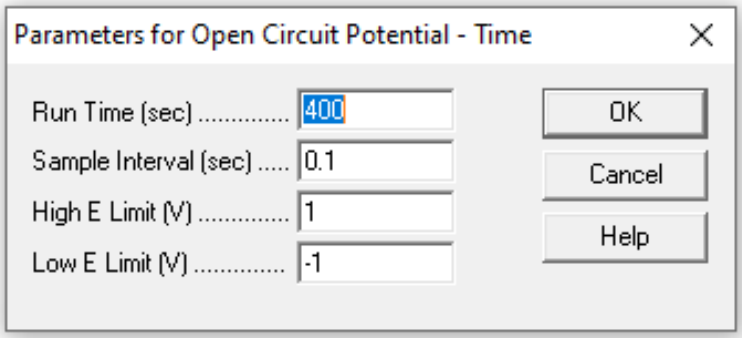

Picture 6: OCP parameters box in the potentiostat CHI 660C.

1.2. Differential Reflectance Spectroscopy (DRS)

DRS, or differential reflectometry, is a technique for analyzing surfaces by using photons (i.e., light varying in wavelengths from near ultraviolet light to visible to infrared light). This interaction occurs between these photons and strongly absorbing materials - metals, alloys, semiconductors, etc. - in the first 10–20 nm. As a result, DRS analyses between 50 and 100 atomic layers of nontransparent solid surfaces. The characteristic probing depth of DRS bridges the gap between surface measurements such as ion scattering, Auger spectroscopy, or ESCA, which probe as deep as 20 monolayers, and XRD, which probes as deep as 1 to 50 mm into a bulk material.[5,6] Two slightly different surfaces are scanned using DRS. The signal thus obtained becomes a "differential reflectogram" that exhibits all of the characteristics of an optical absorption spectrum. Through optical techniques like DRS, it is possible to reveal details about the electronic structure around Fermi surfaces through photon interactions with valence (or conduction) electrons rather than core

electrons. The characteristic energies of electron "interband transitions" serve as an indicator of a material's electron-band structure.

Obviously, DRS can be applied to materials that do not absorb strongly, such as metals, alloys, or semiconductors. Surfaces with transparent or semitransparent surface layers can be identified or characterized as thin-film corrosion products. Due to the difference-forming nature of DRS, it is able to eliminate any undesirable influences that oxides, windows, electrolytes, or instrument variations may have upon a differential reflectogram. Hence, the method is quite sensitive since the signal-to-noise ratio is high.[5,6]

1.3. Spatially & Time-resolved Interfacial Electrochemistry: local *RC* constant: literature review

Since Newman reported the nonuniform distribution of the current density at the inlaid disk electrode, much theoretical and experimental work had been done to explore the current distribution in the electrochemical system and its effects.[7] Smyrl and Newman evaluated several methods measuring the nonuniform current distribution, including direct measurement of the deposit thickness and ring collection efficiencies for the bromide-bromine system.[8,9,10,11] Miller and Bellavance measured the current and potential distribution at rotating disk electrodes by several techniques, including single and double reference probe potential mapping, ring-disk electrode collection efficiency and resistive interaction, interrupter and steady-state resistance measurements, and automatic ohmic compensation methods.[12] Chen et al. developed spatially-resolved ohmic microscopy based on microreference electrodes that can quantitatively measure the ohmic potential across any two points in the electrolyte.[13,14]

An electrochemical cell could be simplified by a representative *RC* circuit, where *R* is the resistance of the electrolyte to the working electrode and *C* is the capacitance of the electrode.

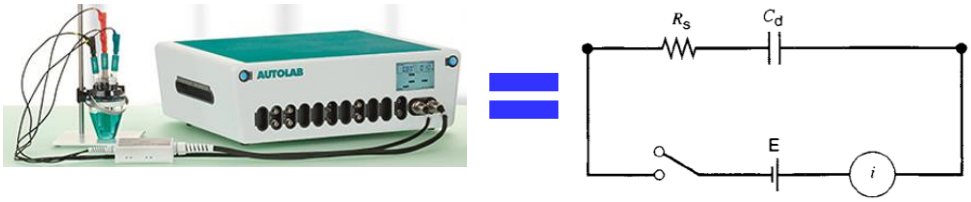

Picture 7: Schematic representation of the RC circuit.

The characteristic time of charging the double layer of the electrode is often regarded as a constant, i.e., *RC* constant.

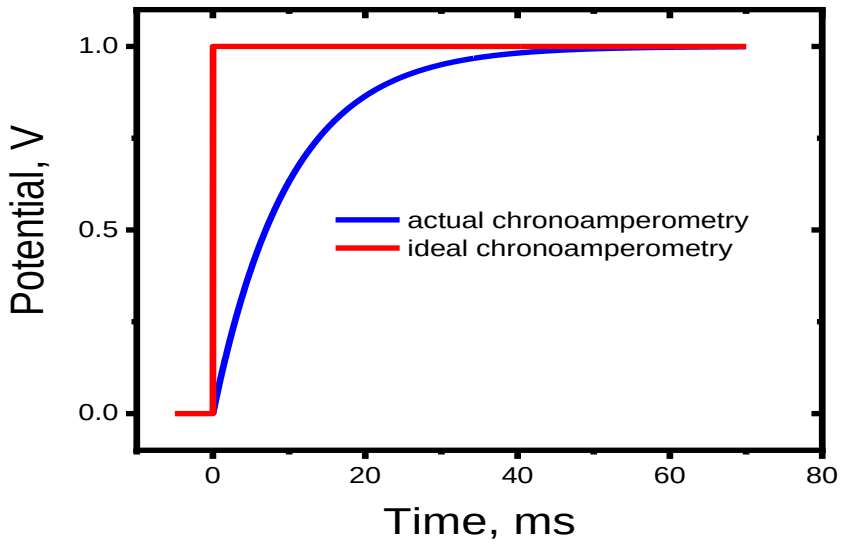

Figure 1: An illustrative chronoamperometry graph.

In fact, when applying a potential in an electrochemical system, it takes a time to reach the expected potential. This time depend mainly on the resistance of the electrolyte. The charge will be accumulated on the surface of the electrolyte and the electrode exactly as it works for a condenser.

Chronoamperometry can be used to measure this time (RC constant in chronoamperometry: Time required to achieve the designated potential (t=R*C)). However, the nonuniform current distribution to the disk electrode indicates the RC constant is a localized parameter instead of being the same for the whole surface. Theoretical calculations by Oldham showed a spatial dispersion of the *RC* constant from zero at the edge to 2 *RC* at the center for the disk electrode.[15]

To the best of our knowledge, the comparison of *RC* constants at the edge and center of a disk electrode has not been realized experimentally. This contribution reports the application of *in situ* differential reflectance spectroscopy (DRS) to semi-quantitatively measure the *RC* constant at the edge and the center of a disk electrode. The result of this finding was reviewed and published in the Journal of Electrochemical Society (*JES*).[16] It was found that localized *RC* constant at the edge is much smaller than that at the center. The edge effect, including the smaller *RC* constant and higher current density, could initiate adsorption/desorption of adsorbates or redox reactions earlier and faster than those at the center, as demonstrated by the controlled stripping of Cu on a gold electrode.

1.4. Application of *RC* constant

- Measuring surface diffusion coefficients of adsorbates
- Electrocatalysis (e.g., CO poisoning Pt catalyst in fuel cell)

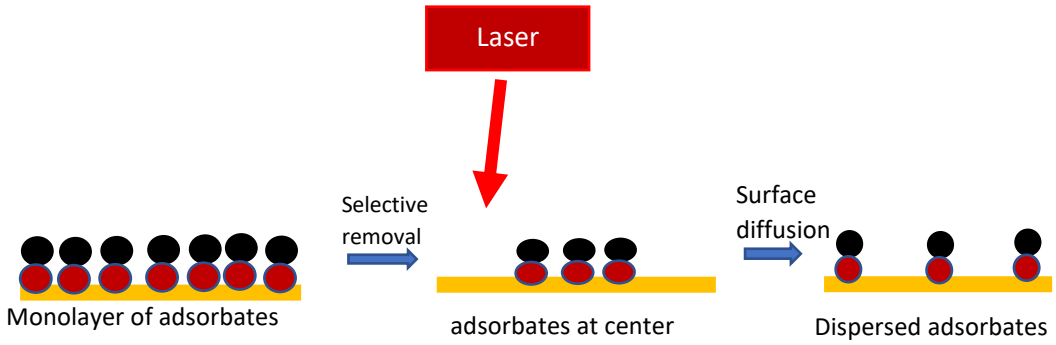

Figure 2: An illustrative removal of adsorbates at the edge of electrode.

1.5. Cementation reaction

Metal cementation occurs when oxidation and reduction occur at the interface of the active metal with the solution containing ions.[17]

1.6. Copper (II)/cobalt cementation reactions

The electrochemical deposition of copper lines/wires on diffusion barrier metals is a vital component of dual damascene interconnect fabrication for integrated circuits. Despite extensive use of this technique for many years, the scaling of integrated circuits features has introduced new challenges in this area. When very high aspect ratio electro-fill features are added to the sub-14 nanometer nodes, the task of void-free bottom-up filling has become remarkably complicated. Using unconventional barriers in Cu interconnects has also led to challenges related to material-specific Cu electrodeposition issues. It remains, however, that electrochemical deposition of Cu^{2+} onto Co is largely underexplored at this time, and it is also accompanied by several technical challenges.

Among these less traditional electrochemical deposition systems, Co (substrate)-Cu^{2+} (deposit) stands out as a specific example, which is the focus of the present study. As diffusion barriers for

Cu^{2+} interconnects are thinned to less than 3 nm, the electrical conductivity of the barrier dramatically drops due to electron scattering. Since Co retains its electrical conductivity at such nanoscale dimensions, Co has become a potentially useful material for this application. Through direct electrochemical deposition of Cu^{2+} on Co, Co is also attractive for this application because it can alleviate the difficulties of high aspect ratio gap-filling. Generally, Cu^{2+} electrochemical deposition is carried out in acidic plating baths, but both the Cu^{2+} seed and the Co substrate corrode or dissolve even in moderately acidic media. To prevent the precipitation of oxidized Cu^{2+} species in alkaline or neutral plating baths, Cu^{2+} complexers are needed. The cathodic shifting potential of electrochemical deposition is caused by these chelating complexes. As a result, electrochemical deposition often moves towards hydrogen evolution reaction (HER), in which hydrogen bubbles adversely affect the electrochemical deposition process.[21,22] However, the spontaneous cementation reaction between copper (II) and cobalt substrate creates an irregular interface when immersed in the copper plating bath of mature copper damascene plating technique.[22,23] It is of utmost importance to investigate the cementation reaction of Cu(II)/Co before electrochemical deposition of Cu^{2+} on the interface between Co substrate newly formed Cu layer.

To date, many similar reactions have been studied for environmental remediation and noble metal production, such as Au(IV)/Zn, Cu(II)/Zn, I_2/Zn, and Cu(II)/Fe.[24-29] and several methods have been reported to measure the kinetics of the cementation reactions, including analysis of the reactant solution, the intersection of the polarization curves, and impedance spectroscopy.[30] One of the most popular techniques reported for determining the rate of the cementation reaction is chronopotentiometry, where the time to consume the reductive substrate is recorded to calculate the rate constant of cementation reaction.[31] The copper (II)/Co cementation reaction via chronopotentiometry by using rotating disk electrodes (RDE) was studied. The reaction rate

constant of the Co reacting with Cu^{2+} and protons was calculated. Then, the impact of deposited Co layer thickness and mass transport was investigated.

2. DIFFERENTIAL REFLECTANCE SPECTROSCOPY MONITORING THE ASYNCHRONOUS TRANSIENT RESPONSE AT THE EDGE AND CENTER OF THE DISK ELECTRODE

2.1. METHODOLOGY

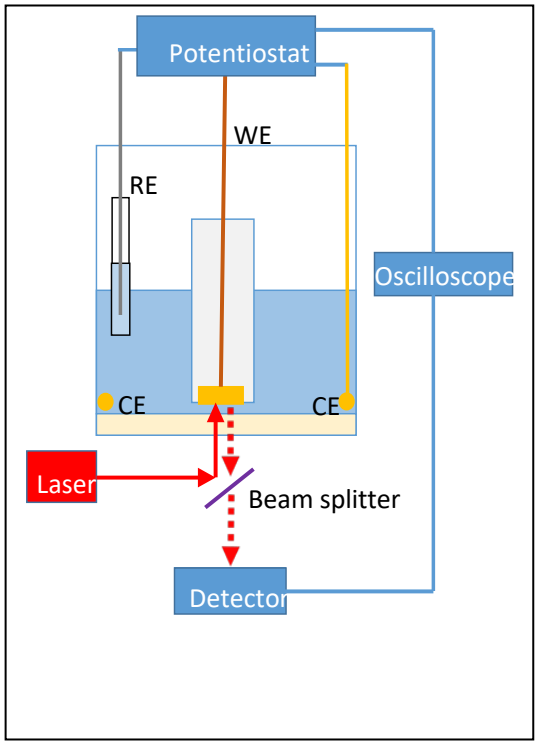

Figure 3: Schematic diagram of in situ DRS experimental set up.

The schematic diagram of the experimental setup for *in situ* DRS is shown in Figure 3. The working electrode (WE) is a gold disk electrode (8 mm, diameter) facing the quartz window.

The counter electrode (CE) is a gold ring (2.5 cm, diameter) made of gold wire (1 mm, diameter). The reference electrode is a reversible hydrogen electrode (RHE). The electrolytes are 0.1 M and 10 mM $HClO_4$ (J.T. Baker Inc., 70 %). The ultrapure water is obtained from a Milli-Q water purification system (>18.0 MOhm-cm). The electrolyte is deaerated by Ar to avoid O_2 interference.

The electrochemical experiment is performed by an Autolab potentiostat (Metrohm USA Inc., PGSTAT302N). A HeNe laser (Thorlabs Inc., 632.8 nm, 21mW) incident on the WE surface is reflected back to the beam splitter through the quartz window before finally measured by the detector (Thorlabs Inc., DET10A2). The potential, current flowing through the working electrode, and optical signal are synchronized and fed into an oscilloscope (Tektronics Inc., TDS684C). Thirty cycles of the raw data are averaged into one spectrum.

Initial test on the controlled stripping of Cu is conducted on a Pt rotating disk electrode (RDE, 5 mm diameter) controlled by Par 616 rotator (Princeton Applied Research). The Polarization curve of copper deposition and stripping is collected in 10 mM $CuSO_4$ (Fisher Scientific, 99 %) and 10 mM $HClO_4$ deaerated by nitrogen. Pt wire is a counter electrode, and Ag/AgCl (3.5 M KCl, BASi Corporate) is the reference electrode. A similar experiment is conducted on the same gold disk electrode immersed in 10 mM $CuSO_4$ and 10 mM $HClO_4$ aqueous electrolyte deaerated by nitrogen. The reference electrode is Ag/AgCl (3.5M KCl), and the CE is the gold ring. The electrochemical experiment is performed on a CH 660C potentiostat (CH Instruments, Inc.).

2.2. RESULTS AND DISCUSSION

2.2.1. In situ DRS and chronoamperometry

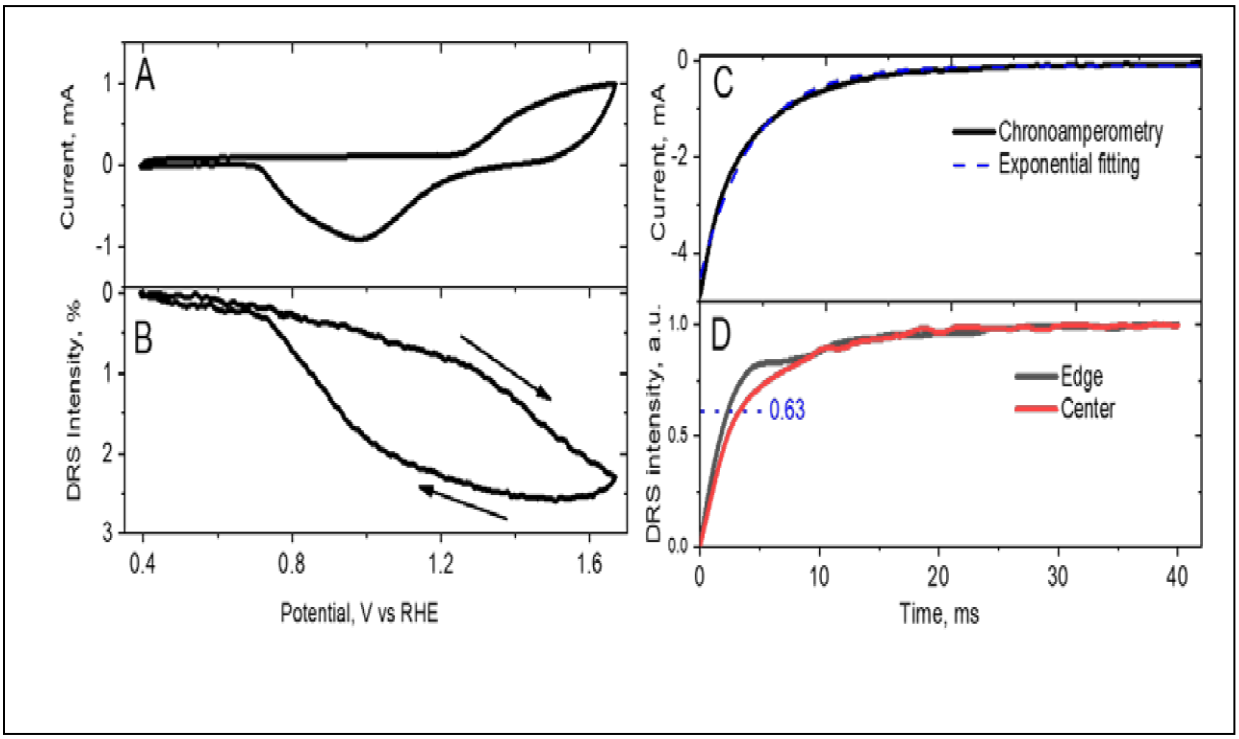

Figure 4: Cyclic voltammogram (Panel A) and in situ DRS (Panel B) collected with an Au disk electrode in 0.1 M $HClO_4$ electrolyte; Chronoamperometry (1.0V-0.4V) and its exponential fitting (black and dashed blue curve, Panel C) and in situ DRS (Panel D) at center (black curve) of the Au electrode.

Shown in panels A and B of Figure 4 are the cyclic voltammetry of the gold electrode sweeping at 1V/s in 0.1 M $HClO_4$ electrolyte and the corresponding reflectance spectrum. The DRS intensity is defined as

$$\frac{\Delta R}{R} = \frac{|R_s - R_{ref}|}{R_{ref}}$$

where R_s is the intensity of reflectance at any potential and R_{ref} is the intensity of reflectance at the reference potential (0.4 V). Overall, $\frac{\Delta R}{R}$ varies in the range of 2.5 % while scanning the potential of the electrode. In the forward scan, $\frac{\Delta R}{R}$ decreases linearly with potential from 0.4 to 1.3 V. A sharper decrease starts at 1.3 V, i.e., the onset of gold oxidation, until the end of gold oxidation reaction at 1.5 V in the backward scan. $\frac{\Delta R}{R}$ resumes back to 0 at 0.4 V after the reduction of gold oxide, indicating the surface is recovered back to the initial state. $\frac{\Delta R}{R}$ at 1 V and 0.4 V are chosen as R_s and R_{ref} in the chronoamperometry since only the double layer charging/discharging occurs, i.e., no redox reactions, resembling a circuit of capacitor and resistor.

Panel C in Figure 4 depicts the current vs. t (*i* vs. t) recorded in a chronoamperometry experiment, where the initial potential is 1.0 V, and the final potential is 0.4 V. Since there is no specific adsorption or redox reaction on the WE, the current could be regarded as the capacitive current of the double-layer charging. The decay of the current is fitted by an exponential function to extract the *RC* constant, which is 4.1 ms. The DRS of the edge (black) and center (red) of the WE shown in Panel D is normalized by setting $\frac{\Delta R}{R} = 0$ at 1.0 V and $\frac{\Delta R}{R} = 1$ at 0.4 V. Both spectra are smoothed by Savitzky-Golay in OriginPro to remove the noise derived from the harmonics of 60 Hz. The time-resolved $\frac{\Delta R}{R}$ follows a similar trend of the current decay, and the time to achieve 0.63 is 2.9 ms and 4.2 ms for the edge and center, respectively. While the *RC* constant (4.1 ms) derived from the chronoamperometry falls between these two values, the difference is not as predicted by Oldham.[15] The offset is mainly due to the semi-quantitative nature of the experimental setup, i.e., the size of the laser beam ($1/e^2$ Beam Diameter 0.7 mm) is relatively large, and the difficulty in locating the center of the laser on the electrode surface accurately.

To clearly show the difference of *RC* constants at the edge and center, we repeated the experiment with 10 mM $HClO_4$ electrolyte, which has a larger resistivity and therefore resulting in a larger *RC*

constant. Shown in Figure 5 is the chronoamperometry and *in situ* DRS of the gold electrode. The *RC* constant of the electrode is determined to be 68 ms by fitting the *i-t* curve (Panel A) with the exponential function. The reflectance spectrum without any smoothing is shown in Panel B, Figure 5. The *RC* constant at the center (red curve) is 142 ms, which is comparable to 2*RC*. The *RC* constant at the edge (black curve) is 51 ms, much smaller than that at the center. *RC* constants at the edge in both 0.1 M and 10 mM $HClO_4$ electrolytes are not zero because the laser covers a large area of the electrode.

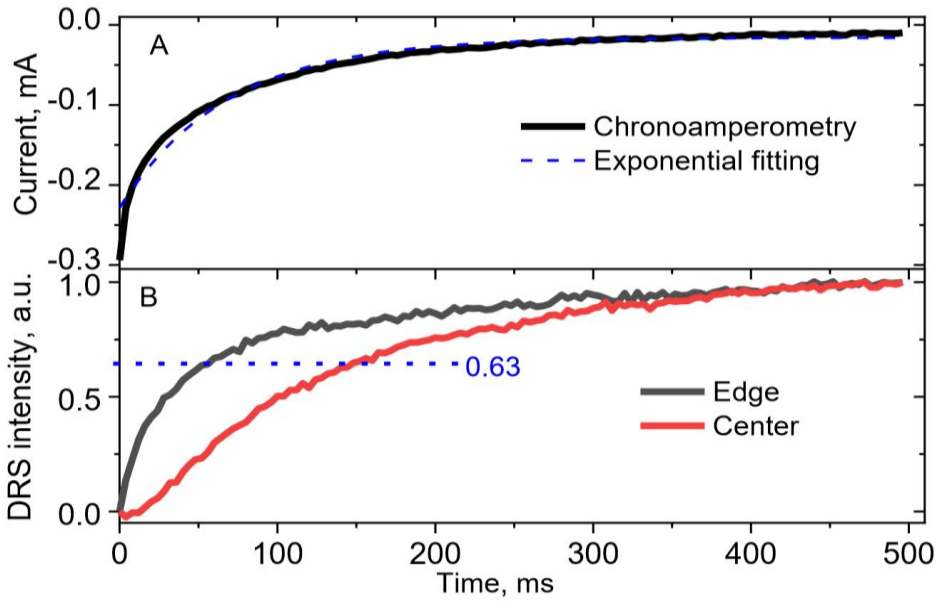

Figure 5: Chronoamperometry (1.0 V-0.4 V) and in situ DRS of the Au electrode in 10 mM $HClO_4$.

2.2.2. Selective removal of Cu on the substrate

The difference in the response time at the edge and the center of the disk electrode provides a basis for selective removal of adsorbates or redox species at the edge of the disk electrode with a series of potential steps of duration like the RC constant. The first experiment is to prove the electrochemical protocol can oxidize the metallic copper deposited on a substrate. We use a Pt rotating disk electrode which provides a quantitatively repeatable copper deposition on RDE, compared to the electrode in the stagnant electrolyte. A layer of Cu is evenly deposited on the Pt RDE at 900 rpm, designated as Cu/Pt electrode.

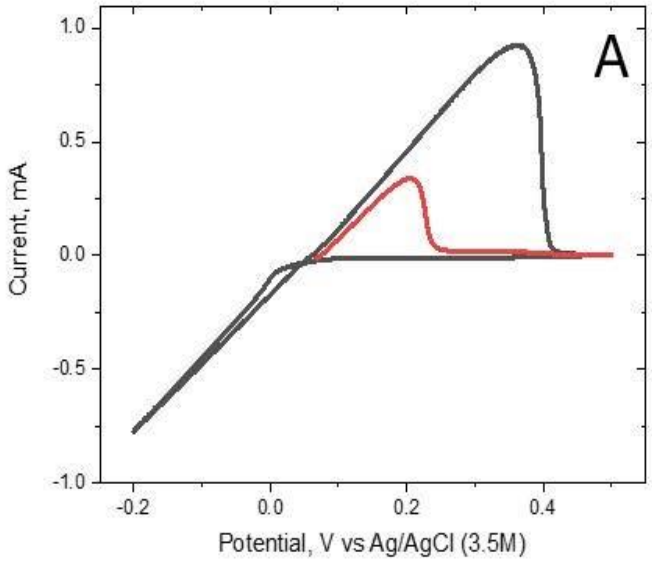

Figure 6: Polarization curve of Pt RDE rotating at 900 rpm in 10 mM $CuSO_4$ and 10 mM and 10 mM $HClO_4$ (black curve) and polarization curve of Cu/Pt electrode after the potential step experiment (red curve).

The black curve in Figure 6, is the polarization curve of the Pt RDE in 10 mM $CuSO_4$ and 10 mM $HClO_4$. The reduction of Cu^{2+} and oxidation of deposited Cu is found to be consistent quantitatively in multiple cycles. After the same amount of Cu is deposited on the Pt RDE, as shown in the black curve, the potential of the electrode is set at 0.05 V, i.e., the potential before Cu oxidation, to obtain a Cu/Pt electrode. A hundred cycles of the potential step from 0.05 V to 1 V (duration of 100 ms) are applied to Cu/Pt electrode to remove the metallic copper. The red curve in Figure 6, is the polarization curve of Cu/Pt electrode scanning from 0.05 V to 0.45 V after the potential step.

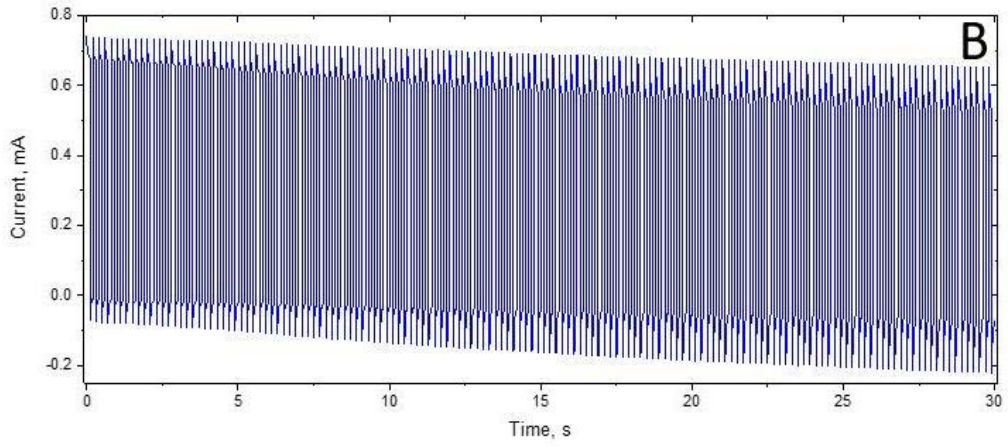

Figure 7: 300 cycles of potential step from 0.05 V to 1.0 V for a duration of 100 ms.

The amount of Cu left on the Pt electrode is about 1/5 of that freshly deposited, indicating a large portion of Cu has been removed by potential steps. Unfortunately, the contrast between the Pt and the Cu thin layer on the Pt electrode is too weak to be observed with a camera, therefore impossible to conclude whether the copper is stripped off the edge of the electrode.

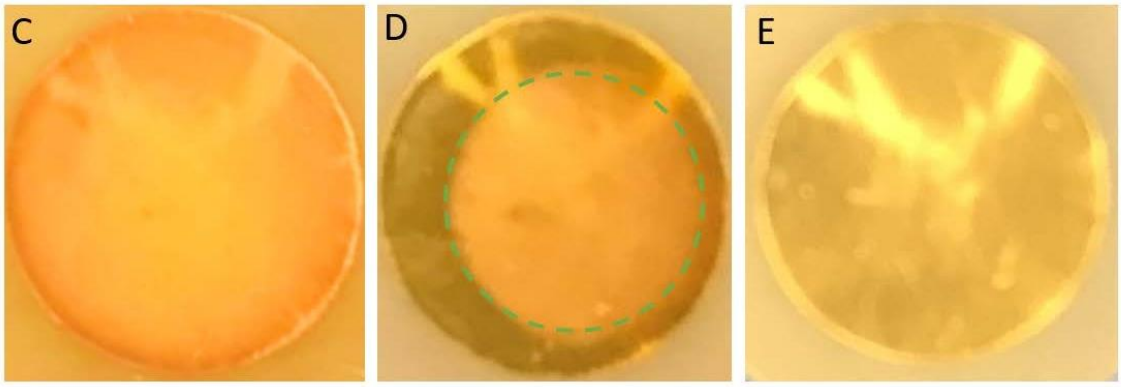

Figure 8: Panel C, Optical image of the Cu/Au electrode; Panel D, partial Cu/Au electrode after potential step; Panel E, bare Au electrode.

To verify the stripping of Cu occurs at the edge, a similar experiment, i.e., Cu deposition and the following stripping by potential steps, is conducted on the gold disk electrode in the same electrolyte. An optical image of the Cu/Au electrode is shown in Panel C, Figure 8. The chronoamperometry (300 cycles) on the electrode is depicted in figure 7, where the magnitude of the oxidation current keeps decreasing in later cycles, indicating less copper is accessible for oxidation in the 100 ms duration. The copper at the edge is removed after the potential steps, and thus bare gold exposed, as shown in Panel D, where the green dashed circle highlights the copper remaining at the center of the electrode. The remaining Cu forms a circle, but its center point does not overlap with that of the Au disk electrode, indicating the configuration of the electrochemical cell is not perfectly symmetrical. A picture of the bare gold electrode is also included for reference (Panel E).

It should be stressed that the root cause of the selective removal of copper is the lower resistance to the edge of the disk electrode. The spatially dependent resistance along the electrode surface results in the varying RC constants and ionic potentials. Local RC constant is the predominant factor for a local site reaching the overpotential to initiate the electrochemical reaction. The electrode is a highly conductive metal and shares the same electric potential anywhere on the surface. Thus, the local surface overpotential, proportional to the kinetics of the reaction, will be determined by the local ionic potential. Therefore, lower ionic potential will result in higher surface overpotential and fast reaction rate at the edge. Overall, both local RC constant and local surface overpotential originated from the unequal resistance at the edge and the center of the disk electrode is responsible for the selective removal of Cu.

3. THE SURFACE KINETICS OF THE COPPER(II)/COBALT CEMENTATION REACTION USING A ROTATING DISK ELECTRODE

3.1. METHODOLOGY

A Pt rotating disk electrode (RDE, 5 mm diameter) is used as the working electrode, and the rotation rate is controlled by a rotator manufactured by Princeton Applied Research. A potentiostat, CHI 660C (CH instrument), is used to control the electrode and run the experiment. For cobalt deposition, a cobalt virgin makeup solution (Co-VMS) is prepared by 50 mM $CoSO_4$ (Fisher Scientific) and 0.5 M boric acid (Fisher Scientific) in ultrapure water (MilliQ). The copper electrolyte for the cementation reaction is prepared by 10 mM $CuSO_4$ (Fisher) and 50 mM Na_2SO_4. A 10 mM H_2SO_4 electrolyte (Fisher Scientific) is prepared to measure the rate constant of the cobalt/proton reaction. All electrolytes are deaerated in the three-chamber cell by nitrogen for 15 mins before the electrochemical measurements.

For cobalt deposition, a cathodic current of 1 mA for designated time via chronoamperometry is applied to the Pt RDE rotating at 700 rpm. The amount of cobalt on the platinum is measured by cyclic voltammetry, and the thickness of the cobalt layer is about 122, 26, 20, and 10 nm.

Once cobalt is deposited on the Pt electrode surface, the Co/Pt electrode is washed by ultrapure water and dried by nitrogen. Co/Pt electrode is moved above another three-chamber cell filled with $CuSO_4/Na_2SO_4$ electrolyte. The electrode is immersed into the electrolyte under different rotational speeds, e.g., 100, 400, and 900 rpm, while the open circuit potential is recorded. The chronopotentiogram recorded will be analyzed to extract the time required for the reaction to complete, t. The kinetics measurements between Co and proton are conducted by immersing the Co/Pt electrode into the 50 mM sulfuric acid electrolyte under the same condition. The

chronopotentiogram is also collected for Co/Pt electrode in a copper plating bath (10 mM $CuSO_4$ and 50 mM H_2SO_4). The potential of the RDE is monitored in all the measurements until stable values are achieved.

3.2. RESULTS AND DISCUSSION

As shown in Figure 9A, it is the chronoamperometry to deposit 122 nm Co on Pt RDE in Co-VMS by passing 1 mA current for 60 s, while the Pt RDE rotary speed is 700 rpm. The potential of the working electrode drops to -1.07 V immediately after the switch is on, and a steady state is reached after 20 seconds of reaction with the solution. The amount of deposited cobalt can be measured by stripping it off at more positive potentials. The polarization curve of Co/Pt electrode collected in the same electrolyte at 50 mV/s is shown in the black curve in panel B, where a peak of cobalt oxidation could be observed. The amount of charge associated with cobalt is calculated to be 34.8 mC by integrating the peak from -0.45 V to 0.65 V. The current efficiency of cobalt deposition is calculated to be 58 %, as it's accompanied by the hydrogen evolution reaction. After the stripping of cobalt, a polarization curve (red curve) is collected on the same electrode. The cathodic current below -0.3 V is the hydrogen evolution reaction on the bare Pt RDE, and no Co oxidation features exist, which indicates all the cobalt has been stripped off in the positive scan of the polarization curve (black curve, Figure 9B).

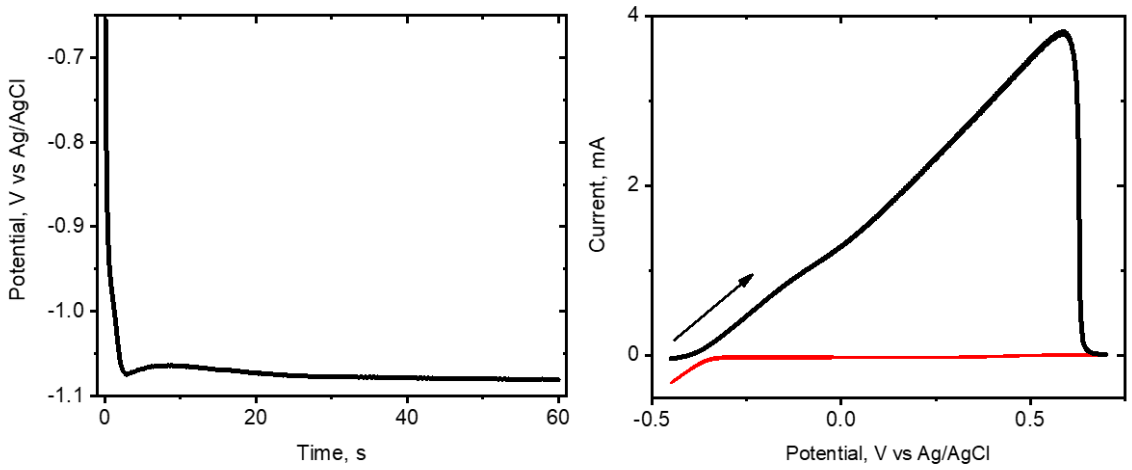

Figure 9: Panel A. chronoamperometry to deposit 122 nm Co on Pt RDE in Co-VMS by passing 1 mA current for 60 s (700 rpm). Panel B. Polarization curve of Co/Pt RDE in VMS (700 rpm, 50 mV/s): 1st cycle (black curve) and 2nd cycle (red curve).

To study the surface reaction, firstly, we investigated the reaction between Co and protons in 50 mM H_2SO_4. Because the copper plating generally involves an acidic bath and the product of the reaction between cobalt and protons, i.e., Co^{2+} and dihydrogen, will diffuse away from the electrode surface, and therefore it can be treated as a pure surface reaction. After cobalt is deposited, the electrode is washed with ultrapure water and dried with nitrogen. The electrode is immersed into the 50 mM H_2SO_4 electrolyte while rotating. As shown in the blue curve of Figure 10 A, the OCP of the Co electrode rotating at 900 rpm stays at negative before a sharp rise at about 130 s to 0.55 V, which is the open circuit potential of Pt in such electrolyte. The transition indicates Co on the surface is corroded into cations and diffused away from the electrode surface. The lower rotation rate will increase the transition time to 156 s and 312 s for 400 and 900 rpm, respectively.

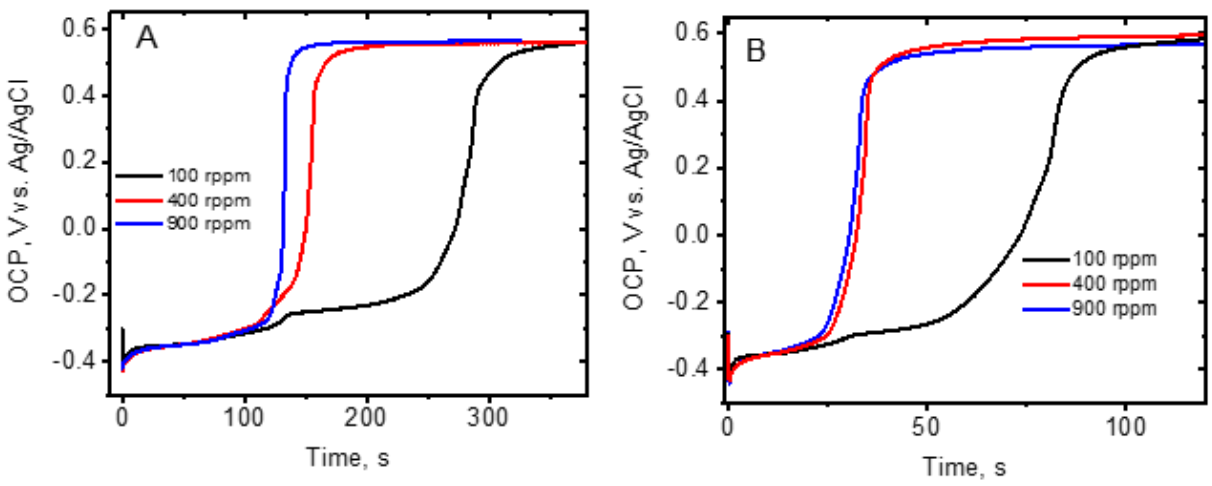

Figure 10: Chronopotentiogram of 122 nm (Panel A) and 26 nm (Panel B) Co film on Pt RDE rotating at 900, 400 and 100 rpm in 50 mM H_2SO_4 (pH=1.45).

The rate of the cementation reaction could be formulated by[30]

$$i_c = \frac{Q}{At} \text{ (Equation 1),}$$

where Q is the amount of Co, A is the geometric surface area of the electrode, and t is the time for the transition between (a) and (b). By applying Faraday's law and the chemical kinetics laws, the rate of the cementation could be formulated by,

$$i_c = nFkC^2 \text{ (Equation 2),}$$

where n is the number of electrons, F is the Faraday constant, k is the rate constant, and C is the concentration of the reactant, i.e., H^+ in this case (pH=1.45). Since the concentration of proton on the electrode surface is unknown, equations 1 and 2 could be combined and rewritten as

$$kC^2 = \frac{Q}{nFAt} \text{ (Equation 3)}$$

The reaction rate, kC^2, is calculated at each rotation rate and plotted versus $\omega^{-\frac{1}{2}}$ as shown in the black symbols and line of Figure 11. A perfect linear relationship is discovered as $kC^2 = -0.000165\omega^{-\frac{1}{2}} + 0.000077$ with R^2 equal to 0.999, which indicates a strong correlation between the rotational speed and the reaction rate. As a matter of fact, a higher rotary speed of electrode in the solution would lead to a thinner diffusion layer and higher concentration of protons on the electrode surface, which would increase the surface reaction rate because of more 'reactant' supplied. When the rotation rate is increased to infinity, $\omega \to \infty$, one could assume the concentration of reaction on the surface is the same as the bulk. In that case, kC^2 is the intercept (0.000077) in the linear fitting as $\omega^{-\frac{1}{2}} \to 0$, and k could be calculated., k is found to be 6.2×10^{-5} $M^{-1}\cdot s^{-1}$ by assuming the reaction of Co and proton is second order.

The effect of the Co thickness is investigated by decreasing the Co thickness down to 26 nm, and chronopotentiogram collected at various rotation rates is shown in Figure 10B. A similar trend is found for 26 nm Co film, e.g., the time required to complete the reaction of Co/H^+ is rotation rate dependent. The reaction rate calculated following Equation 3 for 26 nm Co film is close to that measured by 122 nm film, as shown in Figure 11 (red symbols), indicating a minor impact of the Co thickness for the reaction of Co/H^+. The linear fit of the red symbols results in the following function, $kC^2 = -0.000188\omega^{-\frac{1}{2}} + 0.000082$ with R^2 equal to 0.990, and k calculated from the intercept is found to be 6.5×10^{-5} $M^{-1}\cdot s^{-1}$, which shows a good match with that extracted from 122 nm Co film.

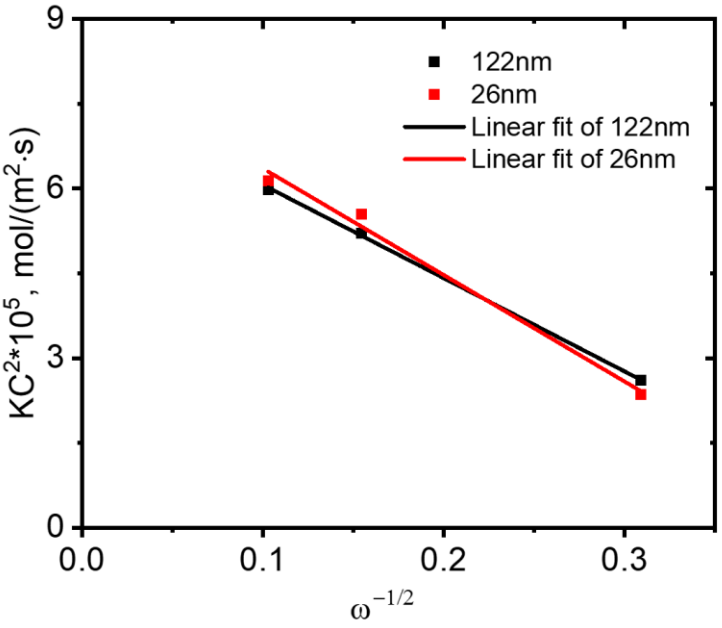

Figure 11: Reaction rate versus $\omega^{-1/2}$ for 26 nm and 122 nm Co film react with 50 mM H_2SO_4. The symbols are the experimental data, and the solid lines are the linear fit.

A 122 nm Co film RDE is immersed into the 10 mM $CuSO_4$/50 mM Na_2SO_4 electrolyte while rotating at various rotation rates. The red curve in Figure 12 is the chronopotentiogram recorded on such an electrode at 400 rpm. It resembles the chronopotentiogram of copper(II)/Zn cementation reaction reported by Xiong and Ritchie.[30] Such a curve could be briefly separated into three stages. At stage (a), Co reacts with Cu^{2+} instantaneously once in contact, and OCP drops from about 0 V to -0.25 V and rise to 0.05 V, representing the complete reaction of Co with Cu^{2+}. A complete layer of Cu covers the surface at the beginning of stage (b), and this layer is gradually converted into copper oxide as the potential rises to 0.1 V (stage (c)). The color of the electrode is brassy and black at stages (b) and (c). The black deposit at stage (c) is not observed in the presence of sulfuric acid, indicating it is the copper oxide that is soluble in acid. The chronopotentiograms collected at 900 rpm (black curve) and 100 rpm (blue curve) resemble that at 400 rpm qualitatively. The transition time, i.e., the time required to complete stage (a), is 39.9 s at 900rpm, 49.9 s at 400 rpm, and 109.0 s at 100 rpm, respectively.

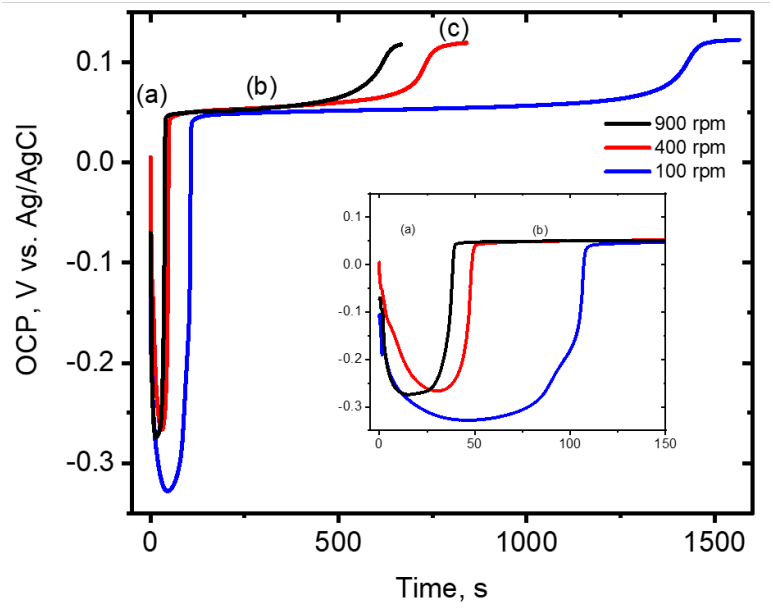

Figure 12: Panel A. Chronopotentiogram of 122 nm Co film RDE rotating at 900 (black curve), 400 (red curve), and 100 rpm (blue curve) in 10 mM $CuSO_4$/50 mM Na_2SO_4; Insert. The enlarged first 150 s of Panel A.

Unlike the reaction of Co/H^+, the product of Co/Cu^{2+} cementation reaction, i.e., metallic copper, will remain on the surface of the electrode. Therefore, the thickness of Co may affect the measurements. The thickness of cobalt film is further reduced to 26 nm. The chronopotentiograms in Figure 13A are collected on 26 nm Co film RDE rotating at 900 (black curve), 400 (red curve), and 100 (blue curve) rpm in 10 mM $CuSO_4$/50 mM Na_2SO_4. Only stages (a) and (b) are shown for clarity. The OCP follows the same trend as these for 122 nm film and the transition time are rotation rate dependent. Since much fewer Co is on the electrode surface for the reaction, the transition time is much shorter for the 26 nm Co film, 11.9 s, 14.8 s, and 39.3 s at 900 rpm, 400 rpm, and 100 rpm, respectively. A comparison of the chronopotentiogram between 26 nm (black curve) and 122 nm (red curve) Co film collected at 100 rpm in 10 mM $CuSO_4$/50 mM Na_2SO_4 is shown in

Figure 13B. Both the stage (a) and (b) are much longer for 122 nm Co film, indicating more bulk Co got involved in the reaction in the thicker Co film.

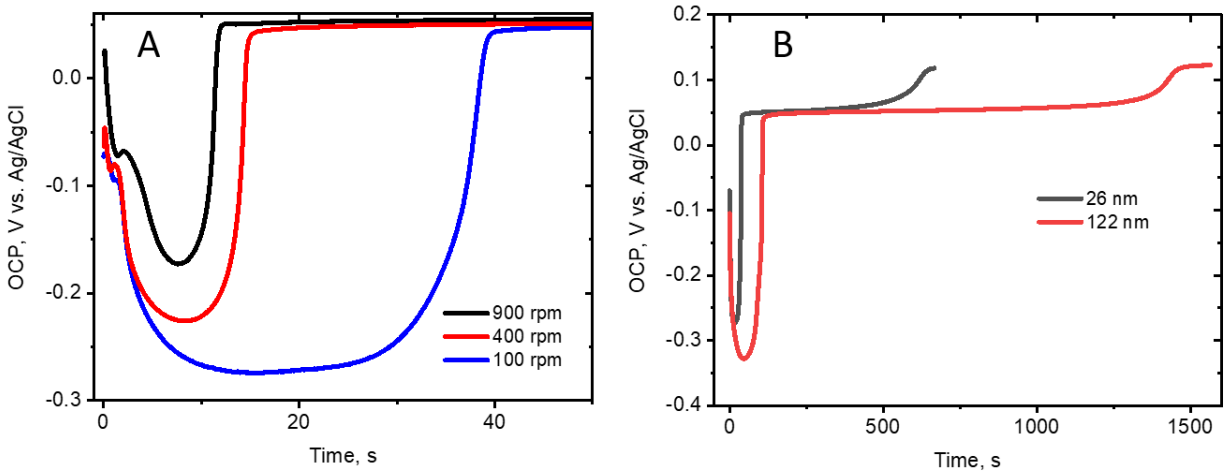

Figure 13: Panel A. Chronopotentiogram of 26 nm Co film on Pt RDE rotating at 900 (black curve), 400 (red curve), and 100 (blue curve) rpm in 10 mM $CuSO_4$/50 mM Na_2SO_4; Panel B. Chronopotentiogram of 26 nm (black curve) and 122 nm (red curve) Co film RDE rotating at 100 rpm in 10 mM $CuSO_4$/50 mM Na_2SO_4.

The cementation reaction between Co and Cu^{2+} can be assumed the first-order reaction, and equation 3 should be revised to the following form[30]:

$$kC = \frac{Q}{nFAt} \quad \text{(Equation 4)}$$

kC is calculated for all the data points collected on 122 nm and 26 nm Co film on the RDE surface and plotted versus $\omega^{-\frac{1}{2}}$ in Figure 14. The reaction rate collected on 122 nm Co film at each rotation rate is larger than that collected on 26 nm thickness Co RDE. It seems to be contrary to the expectation since the porous effect, limiting mass transport in the porous structure of deposit, should be more significant in thicker Co substrate and would lead to longer reaction time in equation 4. The possible reason is the reduced Cu blocked the diffusion of Cu^{2+} to the bulk Co,

and part of Co is preserved in the thick Co layer. However, the total amount of Co calculated in the polarization curve in Figure 9B is still accounted in equation 4. Therefore, thick Co may lead to unreliable kinetics measurements for Co/Cu^{2+} reaction.

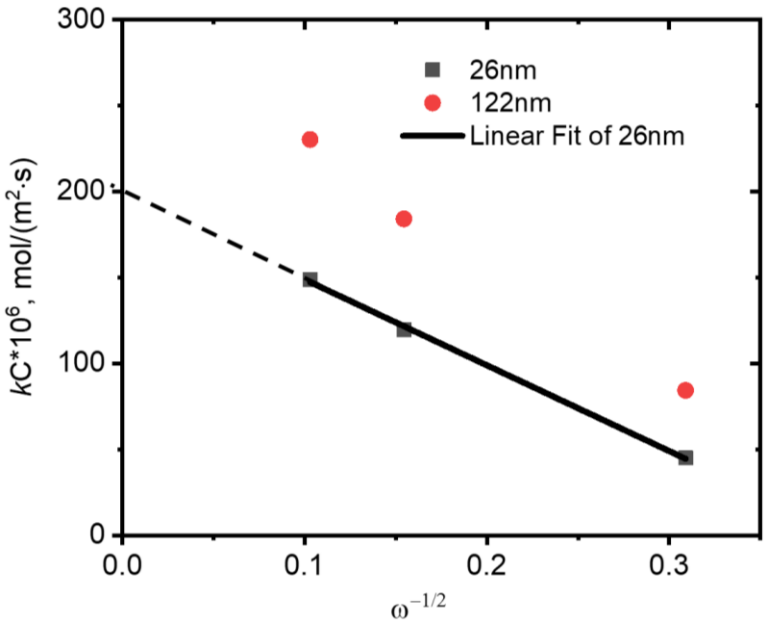

Figure 14: Reaction rate versus $\omega^{-\frac{1}{2}}$ for 26 nm (black) and 122 nm (red) Co film react with 10 mM $CuSO_4$. The symbols are the experimental data, and the solid line is the linear fit.

To investigate the impact of bulk Co on the surface deposition kinetics, we fitted the obtained reaction rate curves, kC - $\omega^{-\frac{1}{2}}$, of the 26 nm case. As shown in figure 14, a linear relationship can be obtained, and its slope indicates that the surface reaction rate will be significantly reduced by decreasing the rotary speed of the electrode. This is because the thickness of the Cu^{2+} mass diffusion layer on the electrode surface is thinner under high rotary speed. Hence, the influence of the mass diffusion layer must be considered in the experiment for surface reaction rate estimation, which becomes negligible only when the RDE rotary speed is high. By using the fitting curve, we

can find *kC* value for 26 nm Co RDE when the rotary speed is infinity (the mass diffusion layer thickness can be treated as zero):

$$kC = -0.000499\omega^{-\frac{1}{2}} + 0.000199 \quad (R^2 = 0.99876) \quad (26\ \text{nm}),$$

The rate constant is 19.9 ± 0.4 μm/s by substituting $\omega^{-\frac{1}{2}} = 0$.

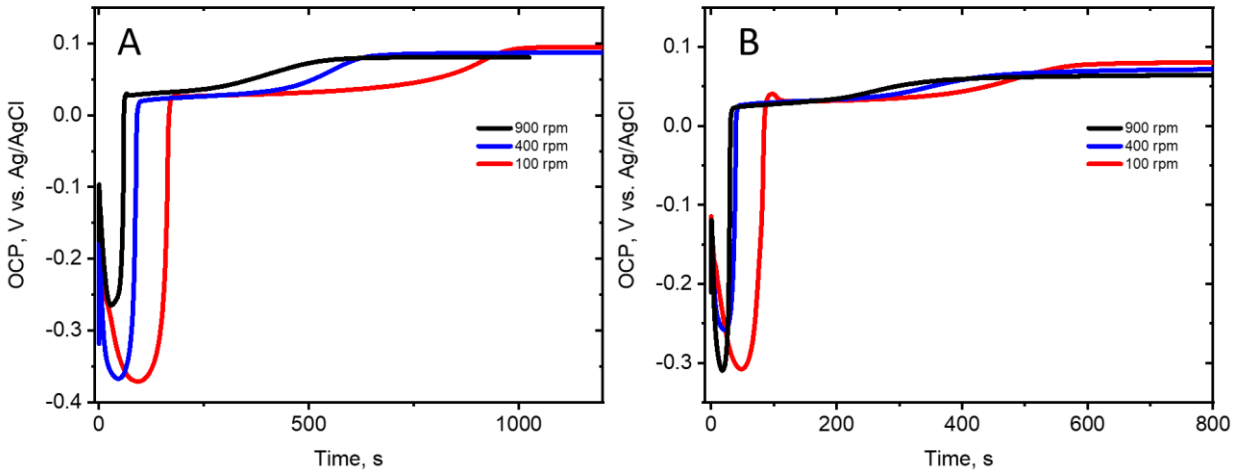

Figure 15: Chronopotentiogram of 20 nm (Panel A) and 10 nm (Panel B) Co film on Pt RDE rotating at 100 (red), 400 (blue) 900 rpm (black), in 1 mM $CuSO_4$/50 mM Na_2SO_4.

Even thinner Co films, e.g., 20 and 10 nm, do not lead to reliable measurements in 10 mM $CuSO_4$/50 mM Na_2SO_4 due to a fast reaction rate, which typically complete in a few seconds.

We further tested the 20 nm and 10 nm Co film in a more diluted Cu^{2+} solution, 1 mM $CuSO_4$/50 mM Na_2SO_4. The chronopotentiogram of 20 nm and 10 nm Co/Pt RDE in 1 mM $CuSO_4$/50mM Na_2SO_4 is similar to the thick Co film in 10 mM $CuSO_4$ qualitatively, as shown in Panel A and B of Figure 15. The reaction rate is calculated according to equation 4 and plotted in Figure 16. The reaction rates measured on 10 nm Co film (black squares) are almost identical to that measured on 20 nm film (red dots) at all rotation rates, indicating the thickness effect is minimized. A linear fit of these symbols leads to the following equations:

$kC = -0.000068\omega^{-\frac{1}{2}} + 0.000030$ (R^2=0.98) for 10 nm Co film, and

$kC = -0.000067\omega^{-\frac{1}{2}} + 0.000029$ (R^2=0.95) for 20 nm Co film.

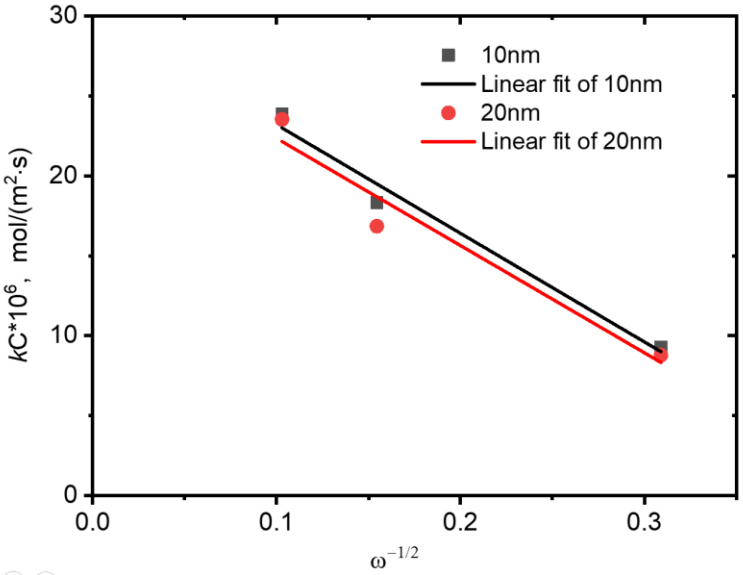

Figure 16: Reaction rate versus $\omega^{-\frac{1}{2}}$ for 10 nm and 20 nm Co film react with 1 mM $CuSO_4$. The symbols are the experimental data, and the solid lines are the linear fit.

The rate constant calculated from the intercept are very close to each other, 30 ± 2 μm/s for 10 nm film, and 29 ± 3 μm/s for 20 nm film. The linearity is not as perfect as thicker Co film, which may be due to the non-uniform deposition of Co films, heterogeneity on the surface.

Since the typical copper plating bath is acidic, we also investigated the cementation reaction of Cu^{2+}/Co in the acidic media. Shown in Figure 17 is chronopotentiogram of 26 nm Co film immersed in the electrolyte containing 10 mM $CuSO_4$/50 mM H_2SO_4 while rotating at 100 rpm. A plateau of the potential is found at about -0.2 V and last for about 5 seconds. The potential rises to 0.05 V in about 12 s, which is much faster than that in $CuSO_4$/Na_2SO_4 electrolyte. This is reasonable since Co also reacts with protons. The potential is maintained at 0.05 V thereafter,

indicating the surface is copper instead of CuO_x. This is also confirmed by the reddish color of the deposited Cu.

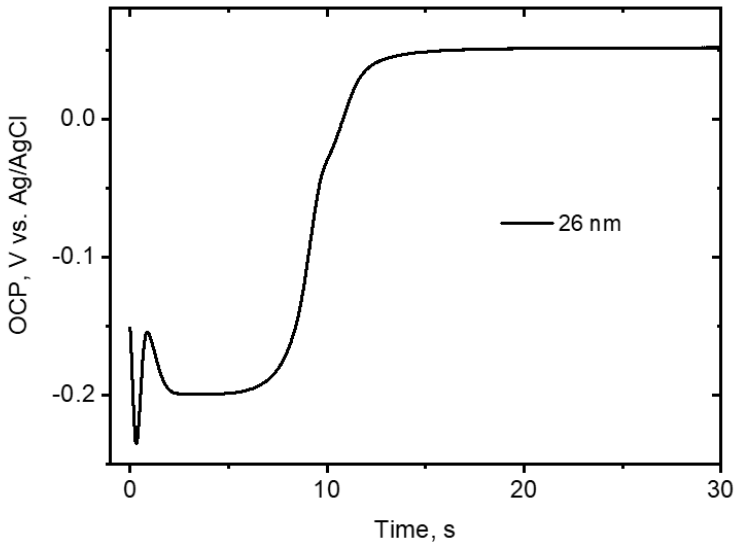

Figure 17: Chronopotentiogram of 26 nm Co film on Pt RDE rotating at 100 rpm in 10 mM $CuSO_4$/50 mM H_2SO_4.

4. CONCLUSION

The nonuniform current distribution on electrode reported by Newton, led to further mathematical calculations demonstrated by Oldham reported that the time to electrodeposit Cu onto electrode is equal to the resistance (R) of the electrolyte multiply by the capacitance (C) due to the electrical charge accumulated on the interface electrolyte and electrode. This time of electrodeposition, represented by RC is a constant. Oldham could mathematically prove that due to the nonuniform current distribution, RC constant at the center is different from RC at the edge. The electrodeposition on the center is 2 times stronger than the deposition at the edge of electrode, therefore 2RC in the center and RC at the edge.

Our challenge was to experimentally demonstrate the assertion reported by Oldham. We purposely designed an electrochemical system to prove the Oldham assertion. We used the Differential Reflectance Spectroscopy to determine the RC constant and the exponential fitting in Chronoamperometry could help calculate the value of RC constants. For the first experiment, we used 10 mM $CuSO_4$ with 0.1 M $HClO_4$, even though the RC constants calculated was different at the edge and the center of the electrode within this electrolyte concentrations, the values of RC constants were not exactly as predicted by Oldham. We repeated the experiment in a less acidic media using a solution of 10 mM $CuSO_4$ with 10 mM $HClO_4$, for this electrolyte concentration, the assertion of Oldham could be proved. In fact, even though the RC constant will remain different at the edge and the center of electrode, the value of RC in the center will not be exactly the double of the RC value at the edge unless you set the resistance of the electrolyte for this purpose. This contribution was reviewed and published in the Journal of Electrochemical Society in October 2021 (*In-situ* Differential Reflectance Spectroscopy Monitoring the Asynchronous Transient

Response at the Edge and the Center of the Disk Electrode[16]). This finding can lay the pathway for many applications in electrocatalysis, selectively removing redox species at the edge of an electrode, measuring surface diffusion coefficients of adsorbates, etc.

Furthermore, we investigated on the Co/Cu^{2+} cementation reaction to contribute on the research regarding the irregular surface created by the electrodeposition of Cu^{2+} on the Co substrate. This technique is well-known as the copper damascene plating technique, used in industry for the manufacturing of small electronic devices such as transistor, micro or nanochips, etc.

So far, not much successful research has been reported to really comprehend the reason of the irregular surface created. Our contribution was to calculate the kinetics between Co/Cu^{2+} and calculate the reaction rate in different conditions.

We used the rotating disk electrode and we clearly demonstrated how the reaction rate between Co and Cu^{2+} is related to the rotation rate of the disk electrode. we found that the thickness of Co substrate reacting with Cu^{2+} has a great influence to successfully determine or calculate the reaction rate of Co/Cu^{2+} cementation reaction. Thinner layer of Co in a more adjusted concentration of Cu^{2+} in solution was the key to successfully determining the reaction. Much other research needs to be done in the future to understand the reason of this irregular surface.

REFERENCES

1. Bard, A.J.; Faulkner, L.R. “Electrochemical Methods: Fundamentals and Applications”, Wiley, New York, **1980**.
2. https://www.sciencedirect.com/topics/chemistry/chronoamperometry#:~:text=4.3%20Chronoamperometry
3. https://www.sciencedirect.com/topics/chemistry/chronopotentiometry
4. https://www.sciencedirect.com/topics/chemistry/open-circuit-potential
5. Hummel, R.E.; Dove D.B.; Holbrook, J. A. “Optical Reflectivity Measurements on Alloys by Compositional Modulation”, *Phys. Rev. Lett.*, **1970**, *25*(5), 290–292.
6. Holbrook, J. A.; Hummel, R.E. “A Differential Reflectometer for Measurements of Small Differences in Reflectivity”, *Rev. Sci. Instrum.*, **1973**, *44*(4), 463–466.
7. Newman, J. *J Electrochem Soc*, **1966**, *113*, 501.
8. Nisancioglu, K.; Newman, J. *J Electrochem Soc*, **1973**, *120*, 1356.
9. Nisancioglu K.; Newman J. *J Electrochem Soc*, **1973**, *120*, 1339.
10. West A.C.; Newman J. *J Electrochem Soc*, **1989**, *136*, 2935.
11. Smyrl W.H.; Newman J. *J Electrochem Soc*, **1972**, *119*, 208.
12. Miller; Bellavance M. I. *J Electrochem Soc*, **1973**, *120*, 42.
13. Chen Y. J.; Belianinov A.; Scherson D. *J Phys Chem C*, **2008**, *112*, 8754.
14. Feng Z. G.; Georgescu N. S.; Scherson D. A. *Russ J Electrochem*, **2017**, *53*, 1003.
15. Oldham K. B. *Electrochem Commun*, **2004**, *6*, 210.
16. Tuala, E. S.; Vasquez, P.; Feng, Z. “in situ DRS Monitoring the Asynchronous Transient Response at the Edge and Center of the Disk Electrode”, *J Electrochem Soc,* **2021**, *50,* pp 1481-1481
17. Strickland P.H.; Lawson F. *Proc. Australas. Inst. Min. Metall*., **1971**, *237***,** 71.
18. Jaskuła M. *Jordan Journal of Earth and Environmental Sciences*, **2009**, *2*, 84.
19. Aktas S. *Hydrometallurgy*, **2010**, *104*, 106.
20. Yahiaoui I.; Aissani-Benissad F. *Arabian Journal of Chemistry*, **2010**, *3*, 187.

21. Lu H.-S.; Wang J.-X.; Zeng X.; Chen F.; Zhang X.-M.; Zhang W.-J.; Qu X.-P. *Electrochemical and Solid-State Letters*, **2012**, *15*, H97.
22. Simpson D. E.; Johnson C. A.; Roy D. *J Electrochem Soc*, **2018**, *166*, D3142.
23. Xu W.-Z.; Xu J.-B.; Lu H.-S.; Wang J.-X.; Hu Z.-J; Qu X.-P. *J Electrochem Soc*, **2013**, *160*, D3075.
24. Parga J. R.; Wan R. Y.; Miller J. D. *Cim Bull*, **1986**, *79*, 82.
25. Ritchie I. M.; Staunton W. P. *J Electrochem Soc*, **1984**, *131*, C100.
26. Ritchie I. M. "Hydrometallurgy 2003 Proceedings", **2003**, *Vols 1 and 2*, 1179.
27. Ahmed A. M. M.; El Adl A. F.; Seleim S. M. *Asian J Chem*, **2013**, *25*, 6711.
28. Nan T. X.; Yang J. G.; Wang W. C.; Li L. C.; Yang J. Y. *T Nonferr Metal Soc*, **2019**, *29*, 1967.
29. Kamimura G.; Matsuura H. *J Sustain Metall*, **2019**, *5*, 341.
30. Xiong J.; Ritchie I. M. "Hydrometallurgy", **1986**, *16*, 301.
31. Zheng J.; Khan M.; LaBrooy S. R.; Ritchie I. M.; Singh P. *J Appl Electrochem*, **1996**, *26*, 509.